# Metal−Organic Frameworks Stabilize Solution-Inaccessible Cobalt Catalysts for Highly Efficient Broad-Scope Organic Transformations

Teng Zhang,[†] Kuntal Manna,[†] and Wenbin Lin[*]

Department of Chemistry, University of Chicago, 929 E. 57th Street, Chicago, Illinois 60637, United States

S *Supporting Information*

ABSTRACT: New and active earth-abundant metal catalysts are critically needed to replace precious metal-based catalysts for sustainable production of commodity and fine chemicals. We report here the design of highly robust, active, and reusable cobalt-bipyridine- and cobalt-phenanthroline-based metal−organic framework (MOF) catalysts for alkene hydrogenation and hydroboration, aldehyde/ketone hydroboration, and arene C−H borylation. In alkene hydrogenation, the MOF catalysts tolerated a variety of functional groups and displayed unprecedentedly high turnover numbers of $\sim 2.5 \times 10^6$ and turnover frequencies of $\sim 1.1 \times 10^5 \text{ h}^{-1}$. Structural, computational, and spectroscopic studies show that site isolation of the highly reactive $(bpy)Co(THF)_2$ species in the MOFs prevents intermolecular deactivation and stabilizes solution-inaccessible catalysts for broad-scope organic transformations. Computational, spectroscopic, and kinetic evidence further support a hitherto unknown $(bpy^{\bullet-})Co^I(THF)_2$ ground state that coordinates to alkene and dihydrogen and then undergoing σ-complex-assisted metathesis to form $(bpy)Co(alkyl)(H)$. Reductive elimination of alkane followed by alkene binding completes the catalytic cycle. MOFs thus provide a novel platform for discovering new base-metal molecular catalysts and exhibit enormous potential in sustainable chemical catalysis.
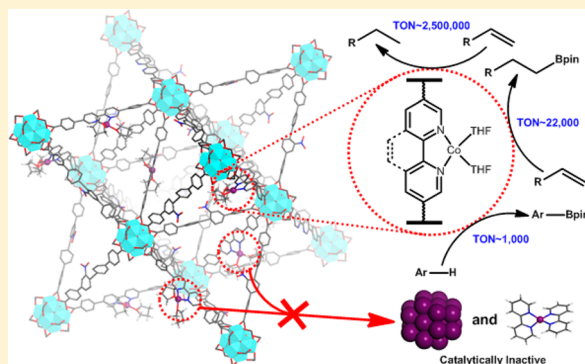
INTRODUCTION

The discovery of new earth-abundant base-metal catalysts is becoming increasingly critical for sustainable and economical production of commodity and fine chemicals owing to the scarcity of precious metals such as Rh, Pd, and Pt. The most common and successful strategy for developing homogeneous base-metal catalysts requires sterically demanding chelating ligands to protect highly active metal centers from intermolecular deactivation into oligomeric species or metal/metal oxide nanoparticles.[1] Such a steric protection strategy can indeed enhance the stability of base-metal catalysts but often at the expense of their catalytic activities.[2] Overly elaborate designs of sterically hindered chelating ligands also make them prohibitively expensive, further reducing the practicality of many elegantly designed homogeneous base-metal catalysts.[3] Alternative strategies are needed for the discovery and development of earth-abundant metal catalysts for sustainable chemical synthesis.

Constructed from metal cluster secondary building units (SBUs) and organic linkers, metal−organic frameworks (MOFs) have emerged as a class of tunable molecular materials with great potential in many applications, including gas storage,[4] separations,[5] sensing,[6] drug delivery,[7] and biomedical imaging.[7b] In particular, MOFs have served as a powerful platform for developing recyclable and reusable single-site solid catalysts.[8] In select examples, MOF catalysts even showed enhanced activities over their homogeneous counterparts.[9] In

this paper, we report the first structural and spectroscopic evidence for a generation of solution-inaccessible base-metal catalysts, achieved by eliminating intermolecular decomposition pathways as a result of active site isolation within a MOF (Figure 1). We show that MOFs can stabilize base-metal homogeneous catalytic species which cannot be prepared in solution, leading to highly active and reusable single-site solid catalysts for a wide range of organic transformations. Our work thus reveals a new MOF-based strategy to discover novel molecular base-metal catalysts and has significant implications in enabling sustainable production of commodity and fine chemicals.

RESULTS AND DISCUSSION

MOF Synthesis and Postsynthetic Metalation with CoCl₂. 2,2′-Bipyridyl (bpy) and derivatives are widely used as chelating ligands with strong binding affinity to base metals, but they do not offer adequate steric protection around the metal centers to afford efficient base-metal catalysts. Inspired by recent reports on precious metal−bpy complex-based MOF catalysts,[9a,10] we surmised that the orthogonal bpy-type ligands comprising the MOF struts are site-isolated and can stabilize base-metal complexes for catalytic organic transformations. Two bpy-containing UiO MOFs, bpy-MOF and bpyv-MOF
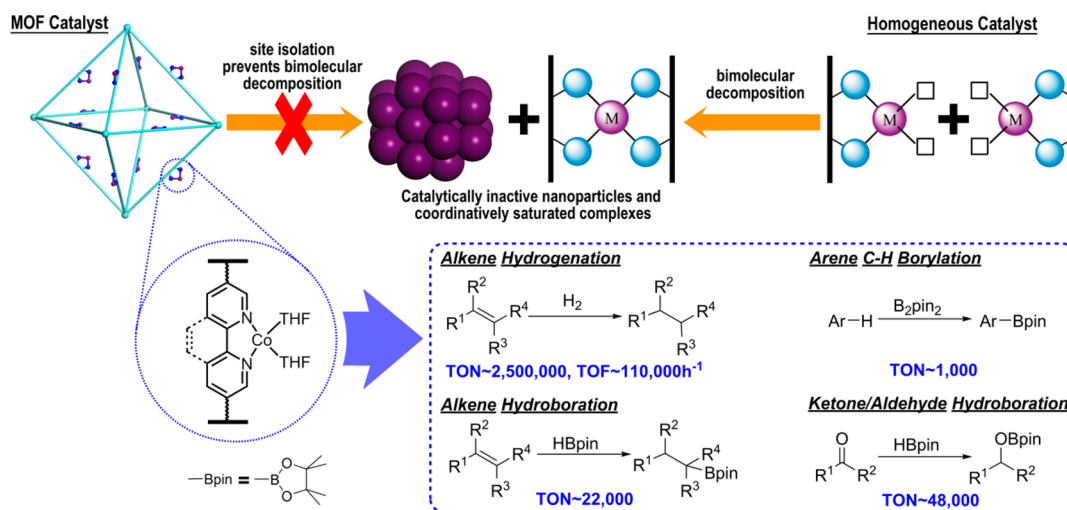
Figure 1. Schematic showing the beneficial effects of active site isolation in MOFs: while homogeneous catalysts undergo intermolecular deactivation via ligand disproportionation/decomposition reactions, such pathways are completely shut down in MOFs due to active site isolation. MOFs thus provide a new platform for discovering novel base-metal molecular catalysts.

(bpyv = 5,5′-bis(carboxyethenyl)-2,2′-bipyridyl), and the mixed ligand MOF, mPT-MOF (PT = 3,8-bis(4-carboxyphenyl)-phenanthryl), were prepared as described previously.[9a,10e,11] The new mixed ligand MOF, mBPP-MOF, was synthesized by heating a mixture of $ZrCl_4$, 4,4′-(2,2′-bipyridyl-5,5′-diyl)-dibenzoic acid (H_2BPP, functionalized ligand), and 4,4′-bis(carboxyphenyl)-2-nitro-1,1′-biphenyl (H_2TPHN, spectator ligand) in the presence of trifluoroacetic acid in dimethylformamide (DMF) at 100 °C. The structure of mBPP-MOF was established by comparison of its PXRD to that of mPT-MOF and TPHN-MOF.[10e] For bpyv-MOF, appearance of several weak extra peaks suggests structure distortion in the powder samples, which has been observed in other nanoscale MOFs.[12] The molar ratios of functionalized and spectator bridging linkers in mPT-MOF and mBPP-MOF were determined to be approximately 1:2 by ${}^1H$ NMR spectra of the MOF digests in a mixture of $K_3PO_4/D_2O/DMSO$-d_6, consistent with the ratios in the synthesis (Figure S1, Supporting Information (SI)).[10e] The TPHN spectator ligand was introduced into mPT-MOF and mBPP-MOF to increase their open channel sizes to facilitate substrate and product diffusion.

Postsynthetic metalation of the MOFs with 8 equiv of $CoCl_2$ afforded MOF-$CoCl_2$ materials as blue-green solids (Figure 2a−c). PXRD patterns showed that all MOF-$CoCl_2$ materials remained crystalline (Figures 2d, and Figures S3, S6a, and S12, SI), whereas inductively coupled plasma-mass spectrometry (ICP-MS) analyses of the digested metalated MOF samples revealed Co loading of 86%, 92%, 63%, and 36% relative to the functionalized bridging ligands for bpy-MOF-$CoCl_2$, bpyv-MOF-$CoCl_2$, mBPP-MOF-$CoCl_2$, and mPT-MOF-$CoCl_2$, respectively. Nitrogen sorption experiments gave BET surface areas of 764, 768, and 1192 m^2/g for bpy-MOF-$CoCl_2$, mBPP-MOF-$CoCl_2$, and mPT-MOF-$CoCl_2$, which are smaller than those of the unmetalated MOFs. However, bpyv-MOF and bpyv-MOF-Co exhibited unexpectedly low BET surface areas of 373 and 294 m^2/g, respectively, which is likely caused by framework distortion upon solvent removal, due to the highly bent nature of the bpyv ligand. Upon metalation, the pore sizes also decreased slightly. The reductions in surface areas and pore sizes of the metalated MOFs are consistent with the presence of Co centers and associated ligands in the MOF cavities.
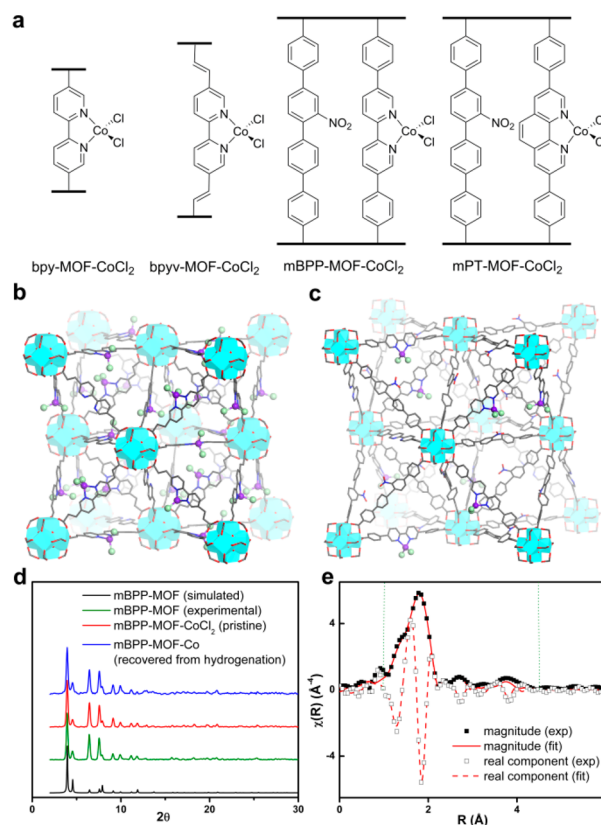

Figure 2. (a) Schematic structures of the MOF-$CoCl_2$ precatalysts. (b, c) Idealized structures of bpyv-MOF-$CoCl_2$ (b) and mBPP-MOF-$CoCl_2$ (c). (d) The similarity of the PXRD pattern simulated from the CIF file of TPHN-MOF (black) and the PXRD patterns of mBPP-MOF (green), mBPP-MOF-$CoCl_2$ (red), and mBPP-MOF-Co recovered from hydrogenation of 1-octene (blue) indicates the retention of mBPP-MOF crystallinity after postsynthetic metalation and catalysis. (e) EXAFS spectra and the fits in R-space at the Co K-edge of bpyv-MOF-$CoCl_2$ showing the magnitude (solid squares, solid line) and real component (hollow squares, dashed line) of the Fourier transform. The fitting range is 1−4.5 Å in R space (within the green dotted lines).

Although earlier reports suggested that the metalated bpy-MOF can adopt ordered structure in a lower-symmetry space group,[10d] this was not observed in our cases, which can be attributed to our mild metalation conditions. Intrinsic disorder and incomplete metalation prevent us from characterizing the MOF-CoCl$_2$ materials by single crystal X-ray diffraction. Instead, we used X-ray absorption spectroscopy (XAS) to investigate the Co coordination environments. Fitting the extended X-ray absorption fine structure (EXAFS) regions of bpy-MOF-CoCl$_2$, bpyv-MOF-CoCl$_2$, mBPP-MOF-CoCl$_2$, and mPT-MOF-CoCl$_2$ X-ray absorption spectra confirmed that the Co centers in the MOFs adopt tetrahedral coordination environments like the model complex Co(^{Me2}bpy)Cl$_2$ (Figures 2e, and Figures S29−32, SI, ^{Me2}bpy = 6,6′-dimethyl-2,2′-bipyridyl).[13]

MOF-Co Materials for Catalytic Alkene Hydrogenation with Unprecedentedly High Activity. Upon treatment with NaBEt$_3$H, MOF-Co materials became highly active catalysts for the hydrogenation of a range of olefins at room temperature (Figure 3a and Table 1).[14] Monosubstituted alkenes such as 1-octene, styrene, and 4-allylanisole were readily hydrogenated within 24 h in quantitative yields using 0.1−0.01 mol % catalysts (entries 1−4 and 8−14, Table 1). At 0.1 mol % Co-loading, bpy-MOF-Co and bpyv-MOF-Co catalyzed hydrogenation of 1,1-, cis-1,2-, and trans-1,2-disubstituted alkenes in 88−100% yields (entries 15−25, Table 1). Additionally, dialkenes such as 1,7-octadiene, and trisubstituted alkenes such as α-terpinene, trans-α-methylstilbene, and 1-methyl-1-cyclohexene, were completely hydrogenated by mBPP-MOF-Co in excellent yields (entries 29, 31−34, Table 1; Table S10, SI). In general, the order of catalytic activity of MOF-catalysts in hydrogenation was mBPP-MOF-Co > mPT-MOF-Co > bpyv-MOF-Co > bpy-MOF-Co (Table S9, SI), due to the decreasing channel sizes in the series. TONs of 2.0×10^5 and 2.1×10^5 were observed for bpyv-MOF-Co and mPT-MOF-Co with 1-octene as the substrate (entries 5 and 6, Table 1), which are higher than those of previously reported Fe- and Co-functionalized salicylaldimine-based MOF catalysts.[9b] Remarkably, mBPP-MOF-Co displayed a TON of 2.5×10^6 in the hydrogenation of 1-octene, which is the highest TON that has ever been reported for Co-catalyzed olefin hydrogenation (entry 7, Table 1). In this case, a turnover frequency of 1.1×10^5 h^{-1} per cobalt center was achieved in the first 9 h, and after simple filtration, the n-octane product contained only 0.26 ppb Co and 1.34 ppb Zr. Moreover, mBPP-MOF-Co-catalyzed hydrogenation of trisubstituted alkenes also proceeded efficiently under milder reaction conditions of 4 atm of H$_2$ and 22 °C (Table S10, SI). MOF-Co catalysts are also tolerant of functional groups. Functionalized alkenes such as allyl acetate, dimethyl itaconate, and 2-vinylpyridine were hydrogenated selectively to propyl acetate, dimethyl 2-methylsuccinate, and 2-ethylpyridine, respectively, in good yields (entries 35−38, Table 1). MOF catalysts were also active in the hydrogenation of tetrasubstituted alkenes, with a TON of 170 observed for the hydrogenation of tetramethylethylene by mBPP-MOF-Co (entry 40, Table 1).

Impressively, at 0.5 mol % Co loading, both bpy-MOF-Co and bpyv-MOF-Co catalysts can be recovered and reused for at least 16 times for the hydrogenation of 1-octene without loss of catalytic activity (Figures S40−42, SI). Complete conversion was observed in every run without olefin isomerization or formation of other byproducts. PXRD patterns of the MOF catalysts after catalysis were identical to those of the pristine
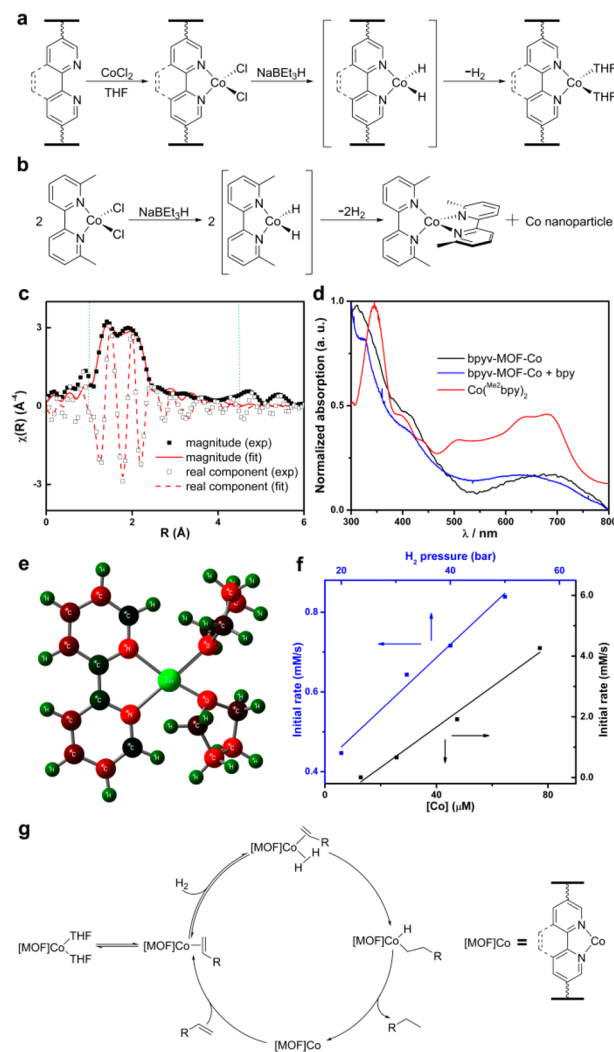

Figure 3. (a) Scheme showing the synthesis of MOF-CoCl$_2$ precatalysts and their reduction by NaBEt$_3$H to form MOF-Co(THF)$_2$ catalysts. (b) Scheme showing the reduction of Co(^{Me2}bpy)Cl$_2$ to the putative (^{Me2}bpy)Co(H)$_2$ which quickly disproportionates to form Co(^{Me2}bpy)$_2$ and Co nanoparticles in solution. (c) EXAFS spectra and the fits in R-space at the Co K-edge of bpyv-MOF-Co(THF)$_x$ showing the magnitude (solid squares, solid line) and real component (hollow squares, dashed line) of the Fourier transform. The fitting range is 1−4.5 Å in R space (within the green dotted lines). (d) UV−vis spectrum of Co(^{Me2}bpy)$_2$ (red), bpyv-MOF-Co (black), and bpyv-MOF-Co(bpy) (blue). (e) Atomic charge distribution of Co(bpy) (THF)$_2$ as calculated by NBO population analysis; atoms bearing positive and negative charges are denoted by green and red colors, respectively. The NBO population analysis suggests a (bpy$^{•-}$)Co^I(THF)$_2$ ground state. (f) Kinetic plots of initial rates (d[ethylbenzene]/dt) for hydrogenation of styrene versus catalyst concentration and hydrogen pressure for the first 120 s, showing first-order dependence on both components. (g) According to the kinetic and computational studies, MOF-Co-catalyzed hydrogenation of alkenes likely proceeds via reversible addition of H$_2$ to (bpy)Co(alkene) followed by turnover-limiting σ-complex-assisted metathesis (σ-CAM).

MOF catalysts, indicating the stability of the framework under catalytic conditions (Figure 2d, and Figures S3, S6, and S12, SI). Additionally, ICP-MS analyses of the organic product showed a negligible metal leaching after the first run, with the leaching of 0.0004% Co and 0.001% Zr for bpy-MOF-Co, 0.0005% Co and 0.002% Zr for bpyv-MOF-Co, and 0.08% Co

Table 1. Catalytic Hydrogenation of Olefins[a]

Entry	Substrate	MOF-Co (mol % Co)	Time	Yield (%)[b]	TONs
1		bpy-MOF-Co (0.1)	20 h	100	>1000
2		bpyv-MOF-Co (0.1)	20 h	100	>1000
3		bpy-MOF-Co (0.01)	20 h	23	2300
4		bpyv-MOF-Co (0.01)	20 h	100	>10000
5		bpyv-MOF-Co (4×10^{-4})	168 h	78	2.0×10^{5}
6		mPT-MOF-Co (3.1×10^{-4})	216 h	66	2.1×10^{5}
7		mBPP-MOF-Co (2.5×10^{-5})	144 h	64	2.5×10^{6}
8		bpy-MOF-Co (0.1)	20 h	100	>1000
9		bpyv-MOF-Co (0.1)	20 h	100	>1000
10		bpy-MOF-Co (0.01)	20 h	15	1500
11		bpyv-MOF-Co (0.01)	20 h	100	>10000
12		mBPP-MOF-Co (0.001)	30 h	100 (91)	>1.0×10^{5}
13		bpyv-MOF-Co (0.01)	48 h	100	>10000
14		mPT-MOF-Co (0.01)	96 h	100 (100)	>10000
15		bpy-MOF-Co (0.1)	20 h	100	>1000
16		bpyv-MOF-Co (0.1)	20 h	100 (95)	>1000
17		mPT-MOF-Co (0.01)	3 h	36	3600
18		mBPP-MOF-Co (5×10^{-4})	32 h	96	1.92×10^{5}
19		mBPP-MOF-Co (0.1)	35 h	100 (99)	>1000
20		bpy-MOF-Co (0.1)	20 h	100	>1000
21		bpyv-MOF-Co (0.1)	20 h	100 (92)	>1000
22		bpy-MOF-Co (0.1)	20 h	88	880
23		bpyv-MOF-Co (0.1)	20 h	100	>1000
24		bpy-MOF-Co (0.1)	20 h	100	>1000
25		bpyv-MOF-Co (0.1)	20 h	100	>1000
26		mBPP-MOF-Co (0.005)	72 h	100	>20000
27		bpyv-MOF-Co (0.01)	48 h	100	>10000
28		mPT-MOF-Co (0.01)	48 h	100	>10000
29		mBPP-MOF-Co (0.005)	48 h	100 (82)	>20000
30		bpyv-MOF-Co (0.1)	24 h	53	530
31		mBPP-MOF-Co (0.1)	36 h	100 (89)	>1000
32		mBPP-MOF-Co (0.1)	96 h	95 (89)	890
33[c]		mBPP-MOF-Co (0.1)	32 h	100 (94)	>1000
34[c]		mBPP-MOF-Co (0.02)	66 h	82	8200
35		bpy-MOF-Co (0.1)	70 h	15	150
36		bpyv-MOF-Co (0.1)	70 h	66	660
37		mBPP-MOF-Co (0.1)	36 h	100	>1000
38		mBPP-MOF-Co (0.1)	48 h	92	920
39[d]		mBPP-MOF-Co (1.0)	24 h	76	76
40[d]		mBPP-MOF-Co (0.1)	60 h	17	170

[a]Reaction conditions: 2−3 mg of MOF-CoCl$_2$, 8 equiv of NaBEt$_3$H (1.0 M in THF) wrt Co, alkene, THF, 40 bar H$_2$, 23 °C. [b]Yields were determined by ^{1}H NMR with mesitylene as the internal standard. Isolated yield in the parentheses. [c]Reaction was performed at 70 °C under 50 bar H$_2$. [d]Reaction was performed at 50 °C.

and 0.1% Zr for mPT-MOF-Co, respectively. A "cross" test further confirmed the heterogeneity of MOF-catalysts: after completely hydrogenating styrene in 6 h, bpyv-MOF-Co was separated from the supernatant. An equal amount of 1-octene was added to the solid and supernatant, respectively. After 18 h under hydrogen atmosphere, 1-octene was completely converted to *n*-octane in the presence of the MOF solid, but no conversion was observed in the presence of the supernatant. This experiment proved that the MOF-Co, not the leached species, was the active catalyst for hydrogenation. Comparisons of the activities of MOF-Co catalysts with those of Co(^{Me2}bpy)Cl$_2$ activated with NaBEt$_3$H and mercury poisoning experiments support that MOF-Co materials are truly single-site solid catalysts with activities several orders of magnitude higher than their homogeneous counterparts (Table S8, SI). In addition, mBPP-MOF-Co gave higher conversion of styrene compared to the analogous bulkier alkene 4-*tert*-butylstyrene under identical conditions, which demonstrates that catalysis is facilitated by Co-sites both inside the pores and on the outside of the MOFs, not the framework surface alone (section 7.7, SI).

Stabilization of Bpy-Co(solvent)$_2$ Species in the MOFs Is Responsible for Catalytic Alkene Hydrogenation. The catalytically active species generated after NaBEt$_3$H treatment of MOF-CoCl$_2$ materials were investigated by comparison with homogeneous analogues using structural, spectroscopic, and computational techniques. Treatment of Co(^{Me2}bpy)Cl$_2$ with 2.0 equiv of NaEt$_3$BH in THF under dinitrogen atmosphere at room temperature afforded a deep blue solution of Co(^{Me2}bpy)$_2$ (0.5 equiv) with the concomitant formation of 1 equiv of H$_2$ and Co nanoparticles as a black precipitate (Figure 3b). Co(^{Me2}bpy)$_2$·^{1}/$_3$THF was crystallized from a concentrated THF/Et$_2$O solution as a paramagnetic bluish-black solid, whose structure was determined by single crystal X-ray diffraction (Figure S16, SI). Presumably, the reductive elimination of H$_2$ from the transient ^{Me2}bpy-cobalt dihydride generates the reduced ^{Me2}bpy-Co species, which undergoes intermolecular ligand-disproportionation to furnish the observed Co(^{Me2}bpy)$_2$ and Co nanoparticles. In a related precedent, the treatment of bulky aryl-substituted bis(imino)pyridine (^{Ar}PDI)-ligated Co-dichloride complex with NaBEt$_3$H resulted in neutral Co-dinitrogen complex (^{Ar}PDI)Co(N$_2$) via reductive elimination of H$_2$ from the putative cobalt(II) dihydride intermediate.[15] The steric protection around the Co center in (^{Ar}PDI)Co(N$_2$) is key to stabilizing the reduced Co compound from undergoing intermolecular decomposition. Co(^{Me2}bpy)$_2$ showed broad UV−vis peaks in THF at 635 and 688 nm, indicating a strong metal-to-ligand charge-transfer (MLCT) transition in this low valence Co species.[16] However, Co(^{Me2}bpy)$_2$ is EPR silent even at 77 K, possibly due to rapid relaxation processes.

Treatment of bpyv-MOF-CoCl$_2$ with NaBEt$_3$H in THF gave bpyv-MOF-Co as a bluish-black solid which was characterized by EXAFS to contain (bpy)Co(THF)$_x$ (93%) and a trace amount of Co nanoparticles (7%). The EXAFS spectrum showed contributions from both Co−N and Co−Co scattering paths, with their bond lengths fitted at 1.96 ± 0.04 Å and 2.45 ± 0.05 Å, respectively (Figure 3c). These bond lengths are consistent with those of Co(^{Me2}bpy)$_2$ and metallic Co, respectively. The ratio for Co−N and Co−Co scattering paths was fitted to be 2:0.9, indicating ∼7% contribution from Co nanoparticles (assuming an average coordination number of

12 as in metallic Co). We believe that the small amounts of Co nanoparticles formed from CoCl$_2$ trapped in the MOF at the metalation step. Control experiments ruled out significant contribution of catalytic activity from the trapped Co nanoparticles (section 4.4, SI).

The bpyv-MOF-Co suspension in THF showed broad absorption peaks at ∼420 nm and ∼700 nm over the scattering background (Figure 3d). Treatment of bpyv-MOF-Co with 2 equiv of 2,2′-bipyridine in THF blue-shifted the absorption peaks to the positions very close to those of the homogeneous Co(^{Me2}bpy)$_2$ complex. Consistent with this, the bpy-stabilized MOF showed greatly reduced activity toward olefin hydrogenation (<17%) and hydroboration (<8%) compared to the original MOF catalyst (section 4.3, SI). In addition, no characteristic band of N≡N was observed in infrared spectroscopy, which rules out the coordination of dinitrogen to Co centers in MOFs. We thus infer the Co coordination environment of (bpy)Co(THF)$_2$ in the MOF-Co material. Density functional theory (DFT) calculations and natural population analyses were performed with the 6-311+G**/B3LYP basis set on (bpy)Co(THF)$_2$ and Co(^{Me2}bpy)$_2$, which show high positive charge distributions on the Co atoms (0.6 and 0.9, Figure 3e), suggesting a (bpy$^{•−}$)Co^I(THF)$_2$ ground state.[16a] XANES spectra show that Co K-edge positions of bpyv-MOF-Co and (^{Me2}bpy)$_2$Co are close to that of Co-(^{Me2}bpy)Cl$_2$ but at energy (by 7−8 eV) significantly higher than that of metallic Co. These results indicate that the Co centers in bpyv-MOF-Co(THF)$_2$ and Co(^{Me2}bpy)$_2$ have higher oxidation states than formally assigned zero valence, consistent with the DFT results. Similar behaviors have been observed for other low-valence transition metal complexes with redox noninnocent ligands.[17]

The spectroscopic, structural, and DFT calculation results indicate that (bpy)Co(THF)$_2$ is likely the active catalyst for hydrogenation reactions. To further investigate the mechanism, the empirical rate law was determined by the method of initial rates (<10% conversion), which shows that the hydrogenation of styrene by mBPP-MOF-Co has a first-order dependence on the catalyst and hydrogen concentrations, and a zeroth-order dependence on the alkene concentration (Figures 3f, and Figure S44, SI). Further DFT calculations were performed to propose a possible catalytic cycle (Figure 3g). In the calculated mechanism, (bpy)Co(THF)$_2$ first binds the alkene reversibly to form a Co(bpy) (alkene) complex. Hydrogen then coordinates to the Co center to form a σ-H$_2$ complex, which undergoes σ-complex-assisted metathesis[18] to form the (bpy)Co(H)(R) species (Figure 3g). Reductive elimination of (bpy)Co(H)(R) in THF forms the alkane product and regenerates the (bpy)Co(THF)$_2$ catalyst. Computation attempts on identifying the transition states gave a five-member ring transition states for the σ-complex-assisted metathesis step with a ΔG‡ = 13.2 kcal/mol (Figures S38 and S39, SI), while a well-defined transition state of the H$_2$ binding step was not found. On the basis of the kinetic and computational results, it can be proposed that the (bpy)Co(alkene) and (bpy)Co(alkene)(H$_2$) intermediates are in pre-equilibrium with the σ-complex-assisted metathesis as the turnover-limiting step.

MOF-Co Materials for Catalytic Hydroboration of Alkenes and Ketones/Aldehydes and Dehydrogenative C−H Borylation of Arenes. MOF-Co materials were also

Table 2. MOF-Co-Catalyzed Hydroboration of Alkenes[a]

Entry	Substrate	Product	MOF-Co (mol % Co)	Time	% Yield[b] (TONs)
1			bpyv-MOF-Co (0.1)	16 h	66 (660)
2			mBPP-MOF-Co (0.1)	18 h	98[c]
3			mBPP-MOF-Co (0.0015)	120 h	81 (54000)
4			mPT-MOF-Co (0.1)	16 h	100 (>1000)
5			mPT-MOF-Co (0.01)	72 h	94[c] (10000)
6[d]			mPT-MOF-Co (0.0025)	144 h	55 (22000)
7			Co nanoparticle (0.1)	20 h	0
8			Co(^{Me2}bpy)Cl$_2$ (0.1)	20 h	37
9			mBPP-MOF (0.1)	24 h	0
10			mPT-MOF-Co (0.1)	16 h	98[c] (>1000)
11			mPT-MOF-Co (0.1)	16 h	92[c] (>1000)
12			mPT-MOF-Co (0.01)	96 h	100 (10000)
13			mPT-MOF-Co (0.1)	48 h	86 (860)
14			mPT-MOF-Co (0.1)	18 h	100 (>1000)
15			mBPP-MOF-Co (0.1)	18 h	100 (>1000)
16[e]			mPT-MOF-Co (1.0)	36 h	82[c]

[a]Reaction conditions: 0.1−0.01 mol % MOF-CoCl$_2$, 10 equiv NaBEt$_3$H (1.0 M in THF), alkene, pinacolborane (1.3 equiv wrt alkene), 23 °C. [b]Yields were determined by ^{1}H NMR with mesitylene as the internal standard. [c]Isolated yield. [d]Reaction was performed at 40 °C. [e]Reaction was performed at 60 °C.
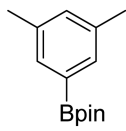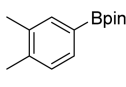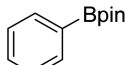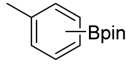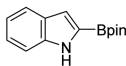
investigated in catalytic hydroboration of alkenes[19] or dehydrogenative C−H borylation of arenes[20] to afford alkyl or arylboronates, which are versatile reagents in organic synthesis. Alkene hydroboration reactions were performed with 0.1−0.01 mol % MOF-Co in a neat mixture of alkene and pinacolborane (HBpin, 1:1.4 molar ratio) at room temperature to afford the desired products in high yields (Table 2). At a 0.1 mol % loading, bpyv-MOF-Co gave complete conversion of 1-octene within 16 h to furnish a mixture of 66% anti-Markovnikov product octylboronate and 34% internal alkenes. However, mix-linker MOF catalysts mPT-MOF-Co and mBPP-MOF-Co afforded pure octylboronate quantitatively under identical conditions. Hydroboration of other terminal alkenes such as 1-decene, 5-methyl-1-hexene and 6-chloro-1-hexene occurred selectively in anti-Markovnikov fashion to afford corresponding alkylboronates with 0.1-0.01 mol % mPT-MOF-Co catalyst in excellent yields (entries 10−13, Table 2). mPT-MOF-Co was also active in catalytic hydroboration of internal alkene and 1,1-disubstituted alkene such as 2-methyl-2-butene and α-methylstyrene. Importantly, mPT-MOF-Co can be recycled at least six times without any loss of activity in

hydroboration of 1-octene. A negligible amount of leaching was observed for Co (0.01%) and Zr (0.03%). No additional hydroboration product was observed after removal of mPT-MOF-Co from the reaction mixture, which rules out any role of leached cobalt species in catalyzing hydroboration. Additionally, Co-nanoparticles and Co(^{Me2}bpy)Cl$_2$/NaBEt$_3$H are barely active in catalyzing hydroboration reactions (entries 7 and 8, Table 2)

The catalytic activity of MOF-Co catalysts in dehydrogenative borylation of aromatic C−H bonds was also investigated. While most efforts have focused on developing borylation catalysts based on Ir(I) complexes,[21] bis(imino)pyridine- and bis(phosphino)pyridine-supported Co catalysts were recently shown to be active for arene C−H borylation.[20] mPT-MOF-Co was initially employed in C−H borylation reactions to optimize reaction conditions such as temperature, MOF activation, borylating agents, and solvents. The screening experiments revealed that the highest yields were obtained when the borylation reactions were performed in neat arene at 100 °C for liquid substrates or refluxed in *n*-heptane at 100 °C for solid substrates. mPT-MOF-Co catalyzed borylation of *o*- and *m*-

xylene selectively at the least sterically hindered C−H bonds. 1,2-Dimethyl-4-(4,4,5,5-tetramethyl-1,3,2-dioxaborolan-2-yl)-benzene and 5-(4,4,5,5-tetramethyl-1,3,2-dioxaborolan-2-yl)-*m*-xylene were obtained from *o*- and *m*-xylene in 90% and 92% yield, respectively, with 0.1 mol % mPT-MOF-Co (entries 3 and 5, Table 3). Although only phenylboronate was afforded
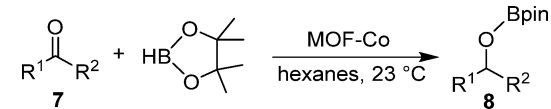
Table 3. MOF-Co-Catalyzed C−H Borylation of Arenes[a]

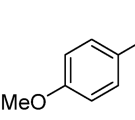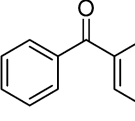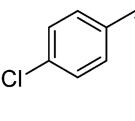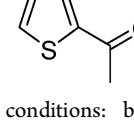| Entry	Product	MOF-Co (mol % Co)	Time	% Yield[b]
1		bpyv-MOF-Co (0.1)	10 d	46
2		mBPP-MOF-Co (0.5)	4 d	50
3		mPT-MOF-Co (0.1)	10 d	100 (92)
4	Bpin	mPT-MOF-Co (1.0)	2.5 d	94
5	Bpin	mPT-MOF-Co (0.1)	9 d	100 (90)
6		mPT-MOF-Co (1.0)	2.5 d	92
7	Bpin	bpyv-MOF-Co (1.0)	11 d	85
8		mPT-MOF-Co (0.1)	8 d	100 (79)
9		mPT-MOF-Co (0.05)	12 d	51
10	Bpin	mPT-MOF-Co (0.1)	6 d	90 (*o*:*m*:*p* = 0:60:40)
11	Bpin	mPT-MOF-Co (0.25)	3 d	100
12		mPT-MOF-Co (0.1)	4.5 d	76
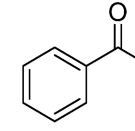
[a]Reaction conditions: 0.25−0.05 mol % MOF-CoCl₂, 10 equiv of NaBEt₃H (1.0 M in THF), arene, B₂pin₂, 100 °C, reflux under N₂. [b]GC yield. Isolated yield in the parentheses.

from benzene as a monoborylated product, the borylation of toluene furnished a mixture of meta- and para-substituted products in a 60:40 ratio. Interestingly, mPT-MOF-Co is at least 125 times more active in C−H borylation of arenes than its homogeneous control PT-CoCl₂ (PT = 1,10-phenanthroline) in terms of TONs. A 1.0 mol % amount of PT-Co afforded 5-(4,4,5,5-tetramethyl-1,3,2-dioxaborolan-2-yl)-*m*-xylene from *m*-xylene in only 8% conversion in 4 days, after which no further conversion was observed with further heating. In contrast, the conversion of *m*-xylene proceeded with time until completion in the presence of 0.1 mol % mPT-MOF-Co (Figure S47, SI). The bpyv-MOF-Co and mBPP-MOF-Co materials were also active in arene borylation reactions, albeit with lower TONs than that of mPT-MOF-Co (entries 1 and 2, Table 3).

The MOF-Co materials were also evaluated for catalytic hydroboration of ketones and aldehydes.[22] The hydroboration reactions were performed by treating ketones or aldehydes with equimolar HBpin in the presence of 0.05−0.01 mol % MOF-Co at room temperature (Table 4). A 0.05 mol % amount of bpyv-MOF-Co afforded borate ester products from a range of carbonyl substrates, including alkyl-, halogen-, and alkoxy-functionalized aryl ketones and aldehydes in essentially quantitative yields. MOF-Co catalysts gave higher TONs in hydroboration of ketones compared to that of the analogous homogeneous catalysts (entries 9 and 10, Table 4). Impressively, a TON of 48000 was obtained for hydroboration of acetophenone with mBPP-MOF-Co (entry 2, Table 4).

Table 4. MOF-Co-Catalyzed Hydroboration of Ketones and Aldehydes[a]

Entry	Substrate	mol % Co	Time	% Yield[b]
1		0.05	1 d	100 (98)
2		0.001	4 d	48[c]
3		0.05	1 d	100 (92)
4	MeO	0.0025	4 d	84
5		0.01	1 d	100 (96)
6	Cl	0.05	1.6 d	100
7		0.01	3 d	84
8		0.05	1 d	100 (96)
9	S	0.01	3 d	41
10		0.05	4 d	62[d]

[a]Reaction conditions: bpyv-MOF-CoCl₂, 10 equiv of NaBEt₃H, carbonyl substrate, hexanes, 23 °C. [b]Yields were determined by ¹H NMR with mesitylene as the internal standard. Isolated yield in the parentheses. [c]Reaction was performed with mBPP-MOF-Co at 40 °C. [d]bpy-CoCl₂ was used as a precatalyst.

Borate ester was also obtained from heterocyclic carbonyl compounds such as 2-acetylthiophene in excellent yields (entries 8 and 9, Table 4). Pure hydroboration products were obtained by simply removing the catalyst via centrifugation followed by removal of the organic volatiles. ICP-MS analyses showed that the amounts of Co and Zr leaching into the supernatant after hydroboration of 4-methoxyacetophenone were 0.02% and 0.008%, respectively, and after filtration, the borylated product contained only 4.2 ppm of Co and 1.3 ppm of Zr.

■ CONCLUSIONS

We have developed highly active, robust, and recyclable single-site base-metal catalysts for alkene hydrogenation and hydroboration, aldehyde/ketone hydroboration, and arene C−H borylation reactions by simple postsynthetic metalation of bipyridyl- and phenanthryl-based MOFs. The MOF catalysts displayed unprecedentedly high turnover numbers (TONs) of up to 2.5×10^6 and turnover frequencies (TOFs) of up to $1.1 \times 10^5 \text{ h}^{-1}$ for alkene hydrogenation. Structural, computational, and spectroscopic studies provide the first direct evidence for the stabilization of highly reactive and solution-inaccessible (bpy)Co(THF)₂ species in MOFs via active site isolation which shuts down intermolecular deactivation pathways. Computational, spectroscopic, and kinetic evidence further support a hitherto unknown (bpy•⁻)Co^I(THF)₂ ground state that coordinates to alkene and then undergoes σ-complex-assisted

metathesis with H$_2$ to initiate catalytic cycles for alkene hydrogenation. This work thus demonstrates for the first time that MOFs enable an entirely new strategy for discovering molecular base-metal catalysts. This novel strategy lifts the constraints placed on traditional homogeneous catalysis and can lead to practical earth-abundant metal catalysts for sustainable chemical catalysis.

■ EXPERIMENTAL SECTION

All of the reactions and manipulations were carried out under nitrogen with the use of standard inert atmosphere and Schlenk techniques or inside a nitrogen-filled glovebox. Crystal structures reported are deposited at the Cambridge Crystallographic Data Centre (CCDC) under deposition numbers 1404664 [Co(^{Me2}bpy)$_2$·$^1/_3$THF] and 1404665 (bpyv-MOF). The crystallographic files can be obtained free of charge. Detailed procedures for the ligand and MOFs synthesis are reported in the Supporting Information.

Synthesis of MOFs and MOF-CoCl$_2$ Precatalysts. In a typical procedure, ZrCl$_4$ (10 mg), H$_2$BPP (6 mg) and 4,4′-bis-(carboxyphenyl)-2-nitro-1,1′-biphenyl (14 mg) were dissolved in 10 mL of DMF, and 0.1 mL of trifluoroacetic acid was added. The solution was heated at 100 °C for 5 days to afford a pale yellow solid which was collected and washed thoroughly with DMF and THF (17 mg, 45% yield). A THF solution of CoCl$_2$ (6 mg) was added to the suspension of mBPP-MOF in THF, and the resultant mixture was stirred overnight, collected, and washed with THF to afford the blue-green mBPP-MOF-CoCl$_2$.

General Procedure for MOF-Co-Catalyzed Olefin Hydrogenation. To a suspension of mBPP-MOF-CoCl$_2$ (1.0 mg, 0.1 mol % Co) in 1.0 mL of THF was added NaBEt$_3$H (10 μL, 1.0 M in THF), and the mixture was stirred for 1 h. The solid was then centrifuged, washed with THF twice, and transferred to a glass vial in 1.0 mL of THF, followed by the addition of α-isopropylstyrene (30 mg, 0.21 mmol). The vial was then placed in a Parr reactor which was charged with 40 bar of hydrogen. After stirring slowly at room temperature for 35 h, the pressure was released, and the MOF catalyst was removed from the reaction mixture via centrifugation and extracted with hexanes twice. The combined organic extracts were concentrated in vacuo to afford pure 1-(3-methylbutan-2-yl)benzene in a quantitative yield.

General Procedure for MOF-Co-Catalyzed Hydroboration of Alkenes. To a suspension of mBPP-MOF-CoCl$_2$ (1.0 mg, 0.1 mol % Co) in 1.0 mL of THF was added 10 μL of NaBEt$_3$H in THF (1.0 M), and the mixture was stirred slowly for 1 h. The solid was centrifuged out of suspension and washed with THF twice. To the solid were added pinacolborane (34 μL, 0.22 mmol) and 1-octene (48 μL, 0.31 mmol). The resultant mixture was slowly stirred at room temperature for 18 h until complete conversion of 1-octene as monitored by GC. The solid was centrifuged out of suspension and extracted with hexane twice. The combined organic extracts were concentrated in vacuo to yield the pure product (52 mg, 0.216 mmol, 98%).

General Procedure for MOF-Co-Catalyzed C−H Borylation of Neat Arenes. To a suspension of mPT-MOF-CoCl$_2$ (3.0 mg, 0.1 mol % Co) in 0.5 mL of THF was added 20 μL of NaBEt$_3$H in THF (1.0 M), and the mixture was stirred slowly for 1 h. The solid was centrifuged out of suspension and washed with THF twice and with m-xylene once. B$_2$pin$_2$ (54.8 mg, 0.216 mmol) in 4.0 mL of m-xylene was added to the vial, and the resultant mixture was transferred to a Schlenk tube. The tube was heated to reflux under nitrogen at 100 °C for 10 d. The reaction mixture was cooled to room temperature, and the solid was centrifuged out of the suspension. The liquid was passed through a short plug of Celite and then concentrated in vacuo to give pure 5-(4,4,5,5-tetramethyl-1,3,2-dioxaborolan-2-yl)-m-xylene (92 mg, 0.396 mmol, 92%).

■ ASSOCIATED CONTENT

⑤ Supporting Information

The Supporting Information is available free of charge on the ACS Publications website at DOI: 10.1021/jacs.6b00849.

> Synthesis and characterization of ligands, MOFs, metalated MOFs, and molecular analogues, procedures for all catalytic reactions, and details for X-ray absorption spectroscopic analysis and DFT calculations (PDF)
> Crystal structure figure and crystallographic file of Co(^{Me2}bpy)$_2$·$^1/_3$THF (CIF)
> Crystal structure figure and crystallographic file of bpyv-MOF (CIF)

■ AUTHOR INFORMATION

Corresponding Author
*wenbinlin@uchicago.edu

Author Contributions
†These authors contributed equally.

Notes
The authors declare no competing financial interest.

■ REFERENCES

(1) (a) Bolm, C.; Legros, J.; Le Paih, J.; Zani, L. *Chem. Rev.* **2004**, *104*, 6217−6254. (b) Enthaler, S.; Junge, K.; Beller, M. *Angew. Chem., Int. Ed.* **2008**, *47*, 3317−3321. (c) Morris, R. H. *Chem. Soc. Rev.* **2009**, *38*, 2282−2291. (d) Sun, C.-L.; Li, B.-J.; Shi, Z.-J. *Chem. Rev.* **2011**, *111*, 1293−1314. (e) Gephart, R. T.; Warren, T. H. *Organometallics* **2012**, *31*, 7728−7752. (f) Tondreau, A. M.; Atienza, C. C. H.; Weller, K. J.; Nye, S. A.; Lewis, K. M.; Delis, J. G. P.; Chirik, P. J. *Science* **2012**, *335*, 567−570. (g) Friedfeld, M. R.; Shevlin, M.; Hoyt, J. M.; Krska, S. W.; Tudge, M. T.; Chirik, P. J. *Science* **2013**, *342*, 1076−1080. (h) Hennessy, E. T.; Betley, T. A. *Science* **2013**, *340*, 591−595. (i) Chen, C.; Dugan, T. R.; Brennessel, W. W.; Weix, D. J.; Holland, P. L. *J. Am. Chem. Soc.* **2014**, *136*, 945−955. (j) Hie, L.; Fine Nathel, N. F.; Shah, T. K.; Baker, E. L.; Hong, X.; Yang, Y.-F.; Liu, P.; Houk, K. N.; Garg, N. K. *Nature* **2015**, *524*, 79−83.

(2) (a) Kundu, S.; Choliy, Y.; Zhuo, G.; Ahuja, R.; Emge, T. J.; Warmuth, R.; Brookhart, M.; Krogh-Jespersen, K.; Goldman, A. S. *Organometallics* **2009**, *28*, 5432−5444. (b) Obligacion, J. V.; Chirik, P. J. *Org. Lett.* **2013**, *15*, 2680−2683.

(3) Gladysz, J. A.; Bedford, R. B.; Fujita, M.; Gabbaï, F. P.; Goldberg, K. I.; Holland, P. L.; Kiplinger, J. L.; Krische, M. J.; Louie, J.; Lu, C. C.; Norton, J. R.; Petrukhina, M. A.; Ren, T.; Stahl, S. S.; Tilley, T. D.;

Webster, C. E.; White, M. C.; Whiteker, G. T. *Organometallics* **2014**, *33*, 1505−1527.

(4) (a) Rosi, N. L.; Eckert, J.; Eddaoudi, M.; Vodak, D. T.; Kim, J.; O'Keeffe, M.; Yaghi, O. M. *Science* **2003**, *300*, 1127−1129. (b) Sumida, K.; Rogow, D. L.; Mason, J. A.; McDonald, T. M.; Bloch, E. D.; Herm, Z. R.; Bae, T.-H.; Long, J. R. *Chem. Rev.* **2012**, *112*, 724−781.

(5) (a) Chen, B.; Liang, C.; Yang, J.; Contreras, D. S.; Clancy, Y. L.; Lobkovsky, E. B.; Yaghi, O. M.; Dai, S. *Angew. Chem., Int. Ed.* **2006**, *45*, 1390−1393. (b) Li, J.-R.; Sculley, J.; Zhou, H.-C. *Chem. Rev.* **2012**, *112*, 869. (c) Yee, K.-K.; Reimer, N.; Liu, J.; Cheng, S.-Y.; Yiu, S.-M.; Weber, J.; Stock, N.; Xu, Z. *J. Am. Chem. Soc.* **2013**, *135*, 7795−7798.

(6) (a) Allendorf, M. D.; Houk, R. J. T.; Andruszkiewicz, L.; Talin, A. A.; Pikarsky, J.; Choudhury, A.; Gall, K. A.; Hesketh, P. J. *J. Am. Chem. Soc.* **2008**, *130*, 14404−14405. (b) Lan, A.; Li, K.; Wu, H.; Olson, D. H.; Emge, T. J.; Ki, W.; Hong, M.; Li, J. *Angew. Chem., Int. Ed.* **2009**, *48*, 2334−2338. (c) Kreno, L. E.; Leong, K.; Farha, O. K.; Allendorf, M.; Van Duyne, R. P.; Hupp, J. T. *Chem. Rev.* **2012**, *112*, 1105−1125. (d) Wanderley, M. M.; Wang, C.; Wu, C.-D.; Lin, W. *J. Am. Chem. Soc.* **2012**, *134*, 9050−9053.

(7) (a) Horcajada, P.; Chalati, T.; Serre, C.; Gillet, B.; Sebrie, C.; Baati, T.; Eubank, J. F.; Heurtaux, D.; Clayette, P.; Kreuz, C.; Chang, J.-S.; Hwang, Y. K.; Marsaud, V.; Bories, P.-N.; Cynober, L.; Gil, S.; Ferey, G.; Couvreur, P.; Gref, R. *Nat. Mater.* **2010**, *9*, 172−178. (b) Della Rocca, J.; Liu, D.; Lin, W. *Acc. Chem. Res.* **2011**, *44*, 957−968.

(8) (a) Zhang, X.; Llabrés i Xamena, F. X.; Corma, A. *J. Catal.* **2009**, *265*, 155−160. (b) Ma, L.; Falkowski, J. M.; Abney, C.; Lin, W. *Nat. Chem.* **2010**, *2*, 838−846. (c) Yoon, M.; Srirambalaji, R.; Kim, K. *Chem. Rev.* **2012**, *112*, 1196−1231. (d) Falkowski, J. M.; Sawano, T.; Zhang, T.; Tsun, G.; Chen, Y.; Lockard, J. V.; Lin, W. *J. Am. Chem. Soc.* **2014**, *136*, 5213−5216. (e) Fei, H.; Shin, J.; Meng, Y. S.; Adelhardt, M.; Sutter, J.; Meyer, K.; Cohen, S. M. *J. Am. Chem. Soc.* **2014**, *136*, 4965−4973. (f) Zhao, M.; Ou, S.; Wu, C.-D. *Acc. Chem. Res.* **2014**, *47*, 1199−1207.

(9) (a) Manna, K.; Zhang, T.; Lin, W. *J. Am. Chem. Soc.* **2014**, *136*, 6566−6569. (b) Manna, K.; Zhang, T.; Carboni, M.; Abney, C. W.; Lin, W. *J. Am. Chem. Soc.* **2014**, *136*, 13182−13185.

(10) (a) Bloch, E. D.; Britt, D.; Lee, C.; Doonan, C. J.; Uribe-Romo, F. J.; Furukawa, H.; Long, J. R.; Yaghi, O. M. *J. Am. Chem. Soc.* **2010**, *132*, 14382−14384. (b) Fei, H.; Cohen, S. M. *Chem. Commun.* **2014**, *50*, 4810−4812. (c) Nickerl, G.; Leistner, M.; Helten, S.; Bon, V.; Senkovska, I.; Kaskel, S. *Inorg. Chem. Front.* **2014**, *1*, 325−330. (d) Gonzalez, M. I.; Bloch, E. D.; Mason, J. A.; Teat, S. J.; Long, J. R. *Inorg. Chem.* **2015**, *54*, 2995−3005. (e) Manna, K.; Zhang, T.; Greene, F. X.; Lin, W. *J. Am. Chem. Soc.* **2015**, *137*, 2665−2673. (f) Øien, S.; Agostini, G.; Svelle, S.; Borfecchia, E.; Lomachenko, K. A.; Mino, L.; Gallo, E.; Bordiga, S.; Olsbye, U.; Lillerud, K. P.; Lamberti, C. *Chem. Mater.* **2015**, *27*, 1042−1056.

(11) (a) Cavka, J. H.; Jakobsen, S.; Olsbye, U.; Guillou, N.; Lamberti, C.; Bordiga, S.; Lillerud, K. P. *J. Am. Chem. Soc.* **2008**, *130*, 13850−13851. (b) Li, L.; Tang, S.; Wang, C.; Lv, X.; Jiang, M.; Wu, H.; Zhao, X. *Chem. Commun.* **2014**, *50*, 2304−2307.

(12) He, C.; Lu, K.; Liu, D.; Lin, W. *J. Am. Chem. Soc.* **2014**, *136*, 5181−5184.

(13) Akbarzadeh Torbati, N.; Rezvani, A. R.; Safari, N.; Saravani, H.; Amani, V. *Acta Crystallogr., Sect. E: Struct. Rep. Online* **2010**, *66*, m1284.

(14) Zhang, G.; Scott, B. L.; Hanson, S. K. *Angew. Chem., Int. Ed.* **2012**, *51*, 12102−12106.

(15) Bowman, A. C.; Milsmann, C.; Atienza, C. C. H.; Lobkovsky, E.; Wieghardt, K.; Chirik, P. J. *J. Am. Chem. Soc.* **2010**, *132*, 1676−1684.

(16) (a) Groshens, T. G.; Henne, B.; Bartak, D.; Klabunde, K. J. *Inorg. Chem.* **1981**, *20*, 3629−3635. (b) Willett, B. C.; Anson, F. C. *J. Electrochem. Soc.* **1982**, *129*, 1260−1266.

(17) Stieber, S. C. E.; Milsmann, C.; Hoyt, J. M.; Turner, Z. R.; Finkelstein, K. D.; Wieghardt, K.; DeBeer, S.; Chirik, P. J. *Inorg. Chem.* **2012**, *51*, 3770−3785.

(18) Perutz, R. N.; Sabo-Etienne, S. *Angew. Chem., Int. Ed.* **2007**, *46*, 2578−2592.

(19) (a) Obligacion, J. V.; Chirik, P. J. *J. Am. Chem. Soc.* **2013**, *135*, 19107−19110. (b) Zhang, L.; Zuo, Z.; Leng, X.; Huang, Z. *Angew. Chem., Int. Ed.* **2014**, *53*, 2696−2700.

(20) Obligacion, J. V.; Semproni, S. P.; Chirik, P. J. *J. Am. Chem. Soc.* **2014**, *136*, 4133−4136.

(21) (a) Cho, J.-Y.; Tse, M. K.; Holmes, D.; Maleczka, R. E.; Smith, M. R. *Science* **2002**, *295*, 305−308. (b) Ishiyama, T.; Takagi, J.; Ishida, K.; Miyaura, N.; Anastasi, N. R.; Hartwig, J. F. *J. Am. Chem. Soc.* **2002**, *124*, 390−391. (c) Mkhalid, I. A. I.; Barnard, J. H.; Marder, T. B.; Murphy, J. M.; Hartwig, J. F. *Chem. Rev.* **2010**, *110*, 890−931. (d) Preshlock, S. M.; Ghaffari, B.; Maligres, P. E.; Krska, S. W.; Maleczka, R. E.; Smith, M. R. *J. Am. Chem. Soc.* **2013**, *135*, 7572−7582.

(22) (a) Locatelli, M.; Cozzi, P. G. *Angew. Chem., Int. Ed.* **2003**, *42*, 4928−4930. (b) Hadlington, T. J.; Hermann, M.; Frenking, G.; Jones, C. *J. Am. Chem. Soc.* **2014**, *136*, 3028−3031. (c) Mukherjee, D.; Ellern, A.; Sadow, A. D. *Chem. Sci.* **2014**, *5*, 959−964.